

# Active Coarse-to-Fine Segmentation of Moveable Parts from Real Images

Ruiqi Wang<sup>1</sup>, Akshay Gadi Patil<sup>1</sup>, Fenggen Yu<sup>1</sup>, Hao Zhang<sup>1</sup>  
<sup>1</sup>Simon Fraser University

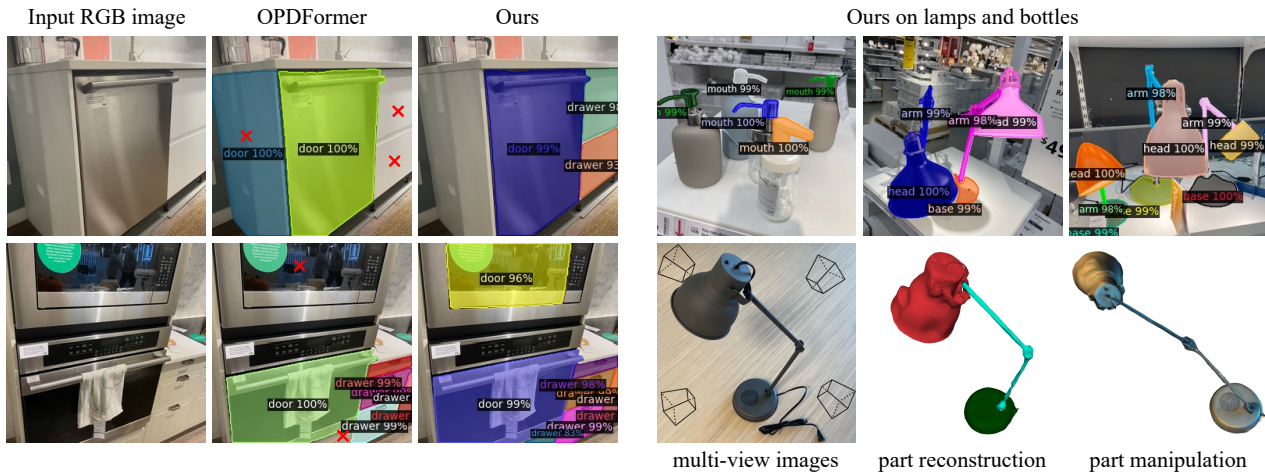


Figure 1. Instance segmentation of moveable parts, with semantic labels, on photos of real-world scenes. Left shows comparison with OPDFormer, the current state of the art, where the small red  $\times$ s indicate erroneous or missed labels. As an application of accurate moveable part segmentations (lamps on top right), we can manipulate 3D reconstructions of articulated objects (Section 7).

## Abstract

We introduce the first active learning (AL) framework for high-accuracy instance segmentation of moveable parts from RGB images of real indoor scenes. As with most human-in-the-loop approaches, the key criterion for success in AL is to minimize human effort while still attaining high performance. To this end, we employ a transformer that utilizes a masked-attention mechanism to supervise the active segmentation. To enhance the network tailored to moveable parts, we introduce a coarse-to-fine AL approach which first uses an object-aware masked attention and then a pose-aware one, leveraging the hierarchical nature of the problem and a correlation between moveable parts and object poses and interaction directions. Our method achieves close to fully accurate (96% and higher) segmentation results, with semantic labels, on real images, with 82% time saving over manual effort, where the training data consists of only 11.45% annotated real photographs. At last, we contribute a dataset of 2,550 real photographs with annotated moveable parts, demonstrating its superior quality and diversity over the current best alternatives.

## 1. Introduction

Most objects we interact with in our daily lives have dynamic moveable parts, where the part movements reflect how the objects function. Perceptually, acquiring a visual and actionable understanding of object functionality is a fundamental task. In recent years, motion perception and functional understanding of articulated objects have received increasing attention in computer vision, robotics, and VR/AR applications. Aside from per-pixel or per-point motion prediction, the *segmentation* of moveable parts serves as the basis for many downstream tasks, including robot manipulation, action planning, and part-based 3D reconstruction.

In this paper, we tackle the problem of *instance segmentation* of moveable parts in one or more articulated objects from RGB images of real indoor scenes, as shown in Figure 1. Note that we use the term articulated objects in a somewhat loose sense to refer to all objects whose parts can undergo motions; such motions can include opening a cabinet door, pulling a drawer<sup>1</sup>, and the movements of a lamp arm. Most prior works on motion-related segmenta-

<sup>1</sup>Strictly speaking, articulated motions are realized by “two or more sections connected by a *flexible* joint,” which would not include the drawer opening motion. However, as has been done in other works in vision and robotics, we use the term loosely to encompass more general part motions.

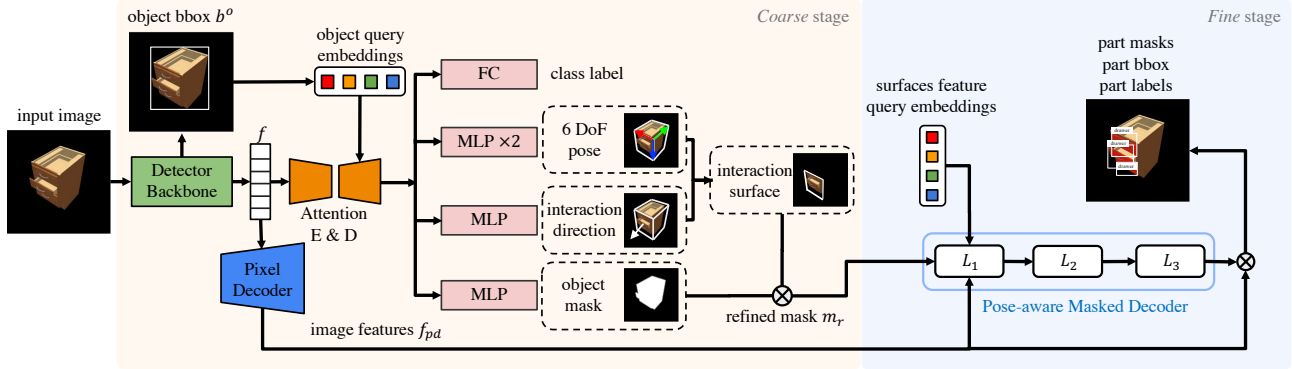


Figure 2. Overview of our pose-aware masked attention network for moveable part segmentation of articulated objects in real scene images. Utilizing a two-stage framework, we first derive a *coarse* segmentation by predicting the object mask, its 6 DoF pose, and the interaction direction, subsequently isolating the interaction surface of the objects. In the *fine* segmentation stage, we combine the object mask and interaction surface to form a refined mask, enabling the extraction of fine-grained instance segmentation of moveable parts.

tions [11, 17, 38] operate on point clouds, which are more expensive to capture than images while having lower resolution, noise, and outliers. Latest advances on large language models (LLMs) have led to the development of powerful generic models such as SAM [16], which can excel at generating quality object masks and exhibit robust zero-shot performance across diverse tasks owing to their extensive training data. However, these methods remain limited in comprehensive understanding of moveable object parts.

To our knowledge, OPD [14], for “openable part detection”, and its follow-up, OPDMulti [28], for “openable part detection for multiple objects”, represent the state of the art in moveable part segmentation from images. However, despite the fact that both methods were trained on real object/scene images, there still remains a large gap between synthetic and real test performances: roughly 75% vs. 30% in segmentation accuracy [28]. The main reason is that manual instance segmentation on real images to form ground-truth training data is too costly. Hence, as a remedy, OPD and OPDMulti both opted to manually annotate 3D mesh or RGB-D *reconstructions* from real-world articulated object scans and project the obtained segmentation masks onto the real images. Clearly, such an indirect annotation still leaves a gap between rendered images of digitally reconstructed 3D models and real photographs, with both reconstruction errors and re-projection errors due to view discrepancies hindering the annotation quality on images.

To close the aforementioned gap by addressing the annotation challenge, we present an *active learning* (AL) [2, 24, 40] approach to obtain high-accuracy instance segmentation of moveable parts, with semantic labels, *directly* on real scene images containing one or more articulated objects. AL is a semi-supervised learning paradigm, relying on human feedback to continually improve the performance of a neural segmentation model. As with most human-in-the-loop approaches, the key criterion for success in AL is to minimize human effort. To this end, we employ a

transformer-based [7] segmentation network that utilizes a masked-attention mechanism [6]. To enhance the network for moveable part segmentation, we introduce a *coarse-to-fine* AL model which first uses an *object-aware* masked attention and then a *pose-aware* one, leveraging the hierarchical nature of the problem and a correlation between moveable parts and object poses and interaction directions.

As shown in Figure 2, in the coarse annotation stage, our AL model with object-aware attention predicts object masks, poses, and interaction directions, so as to help isolate interaction surfaces on the articulated objects. In the fine annotation stage, we combine the object masks and interaction surfaces to predict refined segmentation masks for moveable object parts, also with human-in-the-loop. Unlike prior works on active segmentation [29, 36] which mainly focused on the efficiency of human annotations, our network learns the regions-of-interests (ROIs) from the pose-aware masked-attention decoder for better segmentation sampling in AL iterations in the second stage.

In summary, our main contributions include:

- We introduce the first AL framework for instance segmentation, with semantic labels, of moveable parts from RGB images of real indoor scenes. Our method achieves close to fully accurate (96% and higher) segmentations, with 82% time saving over manual effort, where the training data contains only 11.45% annotated real images.
- Our coarse-to-fine active segmentation model, with both object- and pose-aware masked-attention mechanisms, lead to reduced human effort and improved accuracy in moveable part segmentation over state-of-the-art methods, including OPD [14] and OPDMulti [28].
- Our scalable AL model allows us to accurately annotate a dataset of 2,550 real photos of articulated objects in indoor scenes. We show the superior quality and diversity of our new dataset over current alternatives [14, 28], and the resulting improvements in segmentation accuracy.

## 2. Related Works

**Articulated objects dataset.** The last few years have seen the development of articulation datasets on 3D shapes. Of the many, ICON [10] build a dataset of 368 moving joints corresponding to various parts of 3D shapes from the ShapeNet dataset [5]. The Shape2Motion dataset [32] provides kinematic motions for 2,240 3D objects across 45 categories sourced from ShapeNet and 3D Warehouse [1]. The PartNet-Mobility dataset [35] consists of 2,374 3D objects across 47 categories from the PartNet dataset [21], providing motion annotations and part segmentation in 3D.

All these datasets are obtained via manual annotations and are *synthetic* in nature. Since sufficient training data is made available by these synthetic datasets, models trained on them can be used for fine-tuning on *real-world* 3D articulated object datasets with limited annotations.

Recently, OPD [14] and its follow-up work OPD-Multi [28], provide two 2D image datasets of real-world articulated objects: OPDReal and OPDMulti. In OPDReal, images are obtained from frames of RGB-D scans of indoor scenes containing a single object. OPDMulti, on the other hand, captures multiple objects. Both datasets come with 2D segmentation labels on all *openable* parts along with their motion parameters. However, due to the nature of annotation process, the 2D part segmentation masks obtained via 3D-to-2D projection do not fully cover all openable parts in the image. Also, in OPDReal, objects are scanned from within a limited distance range. Practical scenarios and use cases are likely going to have large camera pose and distance variations. OPDMulti, on the other hand, although incorporates such viewpoint variations, a large portion of this dataset contains frames without any articulated objects [28], which directly affects model training on OPDMulti.

To overcome these limitations, we contribute a 2D image dataset of moveable objects present in the real world (furniture stores, offices, homes), captured using iPhone 12 Pro and 14. We then use our *coarse-to-fine* AL framework (Figure 3 and Section 4) to learn generalized 2D segmentations for moveable object parts.

**Part segmentation in images.** Early approaches [30, 31, 34] to 2D semantic part segmentation developed probabilistic models on human and animal images. While not addressing the 2D semantic part segmentation problem as such, [3, 12, 15, 20, 22] tackled the problem of estimating 3D articulations from human images, which requires an understanding of articulated regions in the input image.

Recently, the development of large visual models, such as SAM [16], has addressed classical 2D vision tasks, such as object segmentation, surpassing all existing models. Such large pre-trained models can be directly employed for *zero-shot* segmentation on new datasets. Follow-up works [8, 43] to SAM aim at multi-modal learning by general-

izing to natural language prompts. For the task of moveable part segmentation in real scene images, we observe an unsatisfactory performance using such models. This is expected since they were never trained on any moveable parts datasets, and therefore, lack an understanding of articulated objects. To our knowledge, OPDFormer [28] is the state-of-the-art that can segment moveable parts in an input image, and is built on the Mask2Former architecture [6]. In our work, we use a transformer architecture in a *coarse-to-fine* manner to obtain moveable part segmentation (Section 4).

**Active learning for image segmentation.** Active learning (AL) is a well-known technique for improving model performance with limited labeled data. This, in turn, allows the expansion of labeled datasets for downstream tasks. Prior works [4, 25–27, 37] have presented different AL frameworks to acquire labels with minimum cost for 2D segmentation tasks. There exist AL algorithms for such tasks [23, 33] that are specifically designed to reduce the domain gap by aligning two data distributions. We cannot borrow such methods to reduce the domain gap between synthetic and real scene images of moveable objects because of the large feature differences (our synthetic images contain no background, unlike real scene images).

More recently, [29, 36] employed AL to refine initial 2D segmentation masks through key point or region selection, requiring little human guidance. Due to potentially multiple moveable parts, such point/region selection is ambiguous for articulated objects. As such, we design an AL framework that reduces manual effort by focusing on: (a) using an improved part segmentation model (Section 4.1), and (b) employing a *coarse-to-fine* strategy (Section 4.2).

## 3. Problem Statement

Given a set of images  $D$  captured from the real-world scene, our input is a single RGB image  $I \in D$  containing one or more articulated objects  $o_i$  from one or more categories  $c_i \in \{\text{cabinet, dishwasher, fridge, microwave, oven, washer}\}$ .

We assume that each object  $o_i$  has more than one moveable parts  $P = \{p_1, \dots, p_k\}$  according to its functionality. Our first goal is to predict the 2D bounding box  $b_i$ , the segmentation mask  $m_i$  represented by a 2D polygon and the semantic label  $l_i \in \{\text{door, drawer}\}$  for each moveable part. Extending the above goal, we also aim to build a labeled image dataset that provides accurate 2D segmentation masks and labels for all  $p_i$ 's, for all  $I \in D$ .

## 4. Method

To address the above problem, we propose an active learning setup that consists of a transformer-based learning framework coupled with a human-in-the-loop feedback process. To this end, we present an end-to-end pose-aware

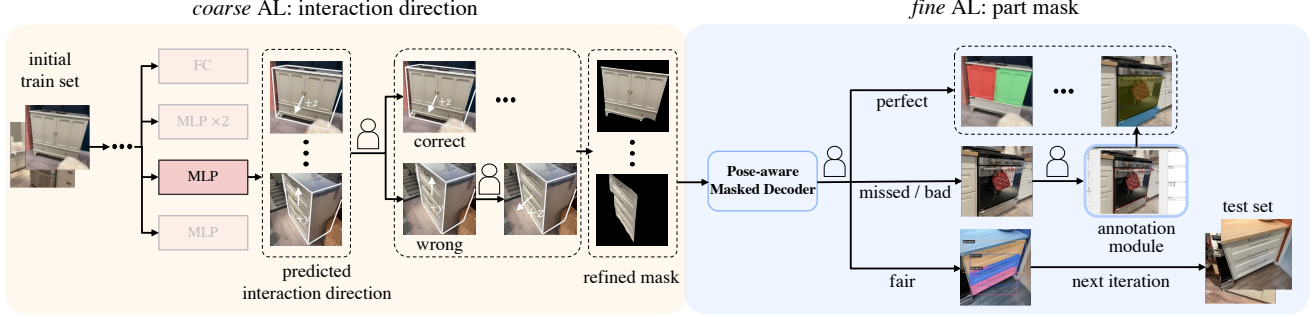


Figure 3. Our coarse-to-fine Active Learning (AL) training pipeline. The *coarse* AL applies on interaction directions and retains high-quality predictions while manually rectifying the rest. These rectified predictions form a constructive prior for refined mask prediction. Subsequently, the *fine* AL stage utilizes these refined masks, employing an iterative training method with continuous human intervention for accurate part mask annotation.

masked-attention network (Fig 2) that works in a *coarse-to-fine* manner for part segmentation and label prediction. By making use of *coarse* and *fine* features from the network, segmentation masks are further refined by humans in the AL setup (Fig 3), resulting in precise moveable part masks.

#### 4.1. Pose-aware masked-attention network

Fig 2 provides a comprehensive depiction of our network architecture, encompassing two distinct stages. In the *coarse* stage, the network processes a single RGB image and computes a refined mask based on outputs from multiple heads, which accurately pinpoints the region containing moveable parts. This stage filters out noise predictions on background and extraneous portions of the object. Subsequently, *fine* stage takes the refined mask and image features to generate part masks, bounding boxes, and semantic labels.

**Coarse stage.** There are three steps in *coarse* stage. First, the input image is passed through a backbone object detector network, producing multi-scale feature maps  $f$  and 2D object bounding boxes  $b^o$ . A pixel decoder [42] upsamples  $f$  for subsequent processing in the *fine* stage. Second, we use a modified version of the multi-head attention-based encoder and decoder [42] to process  $f$ . Inspired by [13], we replace the learned object query embedding with normalized centre coordinates  $(c_x, c_y)$ , width and height  $(w, h)$  from the detected 2D bounding box, enabling the decoder to generate new object query embeddings and estimate 6DoF pose from the 2D bounding box. Third, the decoded queries are passed into multiple MLP heads for (a) object class prediction, (b) 6DoF object pose estimation, (c) object interaction direction and (d) object mask prediction.

We obtain the object class with fully connected layers. For 6DoF pose estimation, we use two identical MLP heads with different output dimensions – one for estimating camera translation  $\tilde{t} = (\tilde{t}_x, \tilde{t}_y, \tilde{t}_z)$ , and the other for estimating the camera rotation matrix  $\tilde{R} \in SO(3)$  as described in [41].

The MLP head for interaction direction prediction outputs a set of possible interaction directions  $d \in$

$\{\pm x, \pm y, \pm z\}$  corresponding to the 6DoF coordinates. Using  $b^o$  and the estimated 6DoF object pose, we can obtain the corresponding 3D *oriented* bounding box  $B^o$ , which tightly fits the  $b^o$ . From among the eight vertices in  $B^o$ , we select vertices of the face along the interaction direction as the representative 2D box for the interaction surface, and use it to crop the input image. This cropped image is further multiplied with the object 2D binary mask to filter out background pixels, obtaining the refined binary object mask  $m_r$ , which guides the subsequent *fine* stage to focus exclusively on the relevant features of the articulated object.

**Fine stage.** There is just one component to this stage, which is the masked-attention decoder from Mask2Former [6] (see Figure 2). It is made up of a cascade of three identical layers,  $L_i$ 's.  $L_1$  takes as input image features  $f_{pd}$  and the refined mask,  $m_r$ , and outputs a binary mask which is fed to the next layer. Eventually, the binary mask at the output of  $L_3$  is multiplied with  $f_{pd}$  resulting in moveable part segmentation in the RGB space. We call this our *pose-aware masked-attention decoder*.

**Loss functions.** We formulate the training loss as below

$$L = L_{class} + L_{dir} + L_{om} + L_{pos} + L_{fine} \quad (1)$$

where  $L_{class}$  is the binary-cross entropy for object class prediction,  $L_{dir}$  is the cross-entropy loss for interaction direction prediction,  $L_{om}$  is the binary mask loss for object mask prediction. We define the loss for pose estimation as  $L_{pos} = \lambda_t L_t + \lambda_{rot} L_{rot}$ , where  $L_t$  is the L2-loss of the translation head and  $L_{rot}$  is the geodesic loss [19] of the rotation head. We set  $\lambda_t$  and  $\lambda_{rot}$  to 2 and 1 respectively. We use a pixel-wise cross-entropy loss for the *fine* stage.

When pre-training, we jointly train our two-stage network in an end-to-end fashion (see Section 6). During fine-tuning on real images with part annotations, we fix MLP weights since ground truth poses and object masks are not available.

Table 1. Dataset statistics across six articulated object categories for OPDReal, OPDMulti and our datasets. Microwave and Oven categories are merged due to their co-occurrence in real scenes. Compared to OPDReal, our dataset is relatively more balanced in terms of sample distribution of different categories, allowing segmentation models to generalize better. OPDMulti does not provide category-wise information, and only 19K out of 64K total images are valid with target and annotation. Parts/img shows the average parts annotated for each image. Our dataset exhibits the most object and part diversity among the three datasets.

		Category					Total	Parts/img
		Storage	Fridge	Dishwasher	Micro.&Oven	Washer		
OPDReal[14]	Objects	231	12	3	12	3	284	2.22
	Images	27,394	1,321	186	823	159	30K	
	image %	91.67%	3.93%	0.62%	2.75%	0.53%	100%	
	Parts	787	27	3	13	3	875	
OPDMulti[28]	Objects	-	-	-	-	-	217	1.71
	Images	-	-	-	-	-	19K/64K	
	Parts	-	-	-	-	-	688	
Ours	Objects	176	51	31	62	13	333	4.33
	Images	925	370	315	775	175	2550	
	image %	36.27%	14.51%	12.35%	30.39%	6.8%	100%	
	Parts	896	159	31	62	13	1161	

## 4.2. Coarse-to-fine active learning strategy

Our active learning setup, consisting of human-in-the-loop feedback, unfolds in a coarse-to-fine manner (see Figure 3). We independently run AL workflow on outputs of both *coarse* and *fine* stages from Section 4.1.

In *coarse* AL part, *Coarse* stage generates predictions for the *test set*. During this phase, users validate interaction direction predictions and rectify inaccuracies. With ground-truth interaction directions established, refined masks  $m_r$  are computed and input into the *fine* stage.

In *fine* AL part, part segmentation mask and label outcome from the *Fine* stage are subject to user evaluation, categorized as perfect, missed, or fair. Specifically: i) A perfect prediction implies coverage of all moveable parts in the final segmentation masks, without any gaps, as well as accurate class labels for each segmented part; ii) A missed prediction effectively refers to a null segmentation mask, and/or erroneous class labels; iii) A fair prediction denotes an output segmentation mask that may exhibit imperfections such as gaps or rough edges, and/or may have inaccuracies in some part class labels. We provide extensive examples of these scenarios in our supplements. During the AL process, perfect predictions are directly incorporated into the next-iteration training set. For all wrong predictions, we employ the labelme [39] annotation interface to manually annotate the part mask polygons, and include such images in the next-iteration training set. Fair predictions, on the other hand, remain in the *test set* for re-evaluation.

The AL workflow on the *fine* stage continues iteratively until all images within the *test set* transition to the training set, becoming well-labeled and eventually leaving the test set vacant. Benefiting from the verified ground-truth interaction direction established in the *coarse* AL part, the *Fine*

stage hones in on features of the target surface, omitting noisy object parts. This streamlined focus notably expedites the annotation process. Further insights into the human verification and annotation procedures will be provided in our supplementary materials.

## 5. Datasets and Metrics

**Datasets.** We use three kinds of real image datasets in our experiments: (1) OPDReal [14], (2) OPDMulti [28], and (3) our dataset. Our dataset images are obtained from the real world by taking photographs of articulated objects in indoor scenes from furniture stores, offices, and homes, captured using iPhone 11Pro, 12, 12Pro and 14. Images are captured with varying camera poses and distances from the objects, and an image can contain more than one object, with multiple moveable parts per object. Differences to OPD and OPDMulti datasets are explained in Section 2.

We consider six object categories – Storage, Fridge, Dishwasher, Microwave, Washer, and Oven. A comparison of dataset statistics is presented in Table 1. OPDReal comprises of  $\sim 30$ K images, with each image depicting a single articulated object. OPDMulti contains  $\sim 64$ K images. Among these, only 19K images are considered “valid”, containing at least one articulated object. Our dataset has a total of 2,550 images, with each image showcasing objects from several categories. We organize our dataset according to the primary object depicted in each image. Our dataset stands out by offering the highest diversity of objects and parts among the compared datasets, including 333 different articulated objects and 1,161 distinct parts.

In terms of the moveable part annotation, both OPDReal and OPDMulti generate annotations on a 3D mesh reconstructed from the RGB-D scans, and project these 3D an-

notations back to the 2D image space to get 2D part masks. This process is prone to reconstruction and projection errors. We, on the other hand, create annotations on the captured images directly using our *coarse-to-fine* active learning framework. See the supplementary material for annotation quality comparisons.

From Table 1, we observe that the majority of data samples in OPDReal belong to the Storage category (91.67%), with the rest (<10%) distributed among the remaining categories. In contrast, our dataset offers a more uniform data distribution across all six categories.

**Metrics.** To evaluate model performance and active learning efficiency, we use the following metrics:

- **Mean Average Precision (mAP):** Following OPD [14], we report mAP@IoU=0.5 for correctly predicting the part label and 2D mask segmentation with IoU  $\geq 0.5$ .
- **Annotation time:** To evaluate the AL setup, we measure manual annotation *and* verification times. For methods without AL, we record the time for labeling only the *test set*, which is the manual annotation time on network segmentation predictions.

## 6. Experiments

We start our experiments by rendering synthetic images from PartNet-Mobility dataset [35] with diverse articulation states, enabling us to obtain sufficient annotations for training 2D segmentation networks and support transfer learning applications. The synthetic dataset contains  $\sim 32\text{K}$  images, evenly distributed across categories, and randomly partitioned into training (90%) and test sets (10%).

We implement our network in PyTorch on two NVIDIA Titan RTX GPUs. All images are resized to  $256 \times 256$  for training. During pre-training on the PartNet-Mobility dataset, we use the Adam optimizer with an initial learning rate ( $lr$ ) of  $2.5e-4$ , reducing it by a factor of  $\gamma = 0.1$  at 1K and 1.5K epochs separately over a total of 2K epochs. When fine-tuning on real images, we use the same  $lr$  and  $\gamma$  at 3.5K and 4K epochs over a total of 4.5K epochs.

### 6.1. Competing methods

We compare our active *coarse-to-fine* part segmentation model with three 2D segmentation methods and also analyze two variants of our proposed approach.

- **Grounded-SAM** [8], which combines Grounding-DINO [18] and Segment Anything [16], is a large visual model that can be used for zero-shot 2D object detection and segmentation, and supports text prompts.
- **OPD-C** [14], which is the first work for detecting openable parts in images based on MaskRCNN [9].
- **OPDFormer-C** [28], a follow-up of OPD-C based on Mask2Former [6], is the state-of-the-art for openable part segmentation of multiple articulated objects in images.

Table 2. Quantitative comparison against competing segmentation methods and variants of our method. In the table, “AL” indicates whether the method uses active learning. “Time” column represents the annotation time metric described in Section 5.

Method	AL	segm mAP $\uparrow$	Time (hr) $\downarrow$
Grounded-SAM[8]	-	22.9	35.5
OPD-C[14]	-	46.4	28.3
OPDFormer-C[28]	-	71.8	16.3
Ours <sub>w/oAL</sub>	-	82.1	13.4
Ours <sub>f-AL</sub>	✓	96.6	7.5
Ours	✓	<b>96.7</b>	<b>6.5</b>

Table 3. Ablation study on our key components.

Row ID	Obj.	Pos.	Dir.	AL	segm mAP $\uparrow$	Time (hr) $\downarrow$
1	-	-	-	-	71.8	16.3
2	✓	-	-	-	74.6	15.1
3	✓	✓	✓	-	82.1	13.4
4	✓	-	-	✓	92.4	8.1
5	-	✓	✓	✓	96.2	7.3
6	✓	✓	✓	✓	<b>96.7</b>	<b>6.5</b>

- **Ours<sub>w/oAL</sub>** is a variant that does not use human feedback – it infers part segmentation results based only on the transformer-based model.
- **Ours<sub>f-AL</sub>** is variant of our approach that uses only the *fine* stage of the AL framework. That is, verification and annotation of just the part masks is done.

### 6.2. Evaluation on Our Dataset

We split our dataset into 550/2000 as train/test sets and evaluate the performance of all competing methods on our *test set*. Note that all methods, except Grounded-SAM, undergo fine-tuning on our *train set*. Figure 6 shows qualitative results of different methods on our *test set*.

**Quantitative comparison.** Table 2 compares four non-AL methods. Among these, Grounded-SAM has the lowest performance due to its direct evaluation on the *test set* without fine-tuning. Its poor performance also shows that current large AI models are still limited in understanding object parts without adequate training on well-labeled data. Conversely, Ours<sub>w/oAL</sub> model, fine-tuned on our *train set*, outperforms competing methods, achieving  $>80\%$  segmentation mAP. The architectural designs of OPD-C and OPDFormer, based respectively on vanilla MaskRCNN and Mask2Former, are tailored for universal segmentation tasks. Therefore, they inadequately address the unique characteristics of articulated objects, whose movable parts are closely tied to object pose and interaction directions. In contrast, our approach effectively leverages the hierarchical structure of the scene, object, and part present in the input image, resulting in a much better performance. Beyond accuracy metrics, we observe that all non-AL methods require significant human effort for labeling the *test set*. This is mainly

Table 4. Quantitative comparison against competing segmentation methods and our model variant on OPDReal, OPDMulti test set.

	segm mAP ( $\uparrow$ )			
	Grounded-SAM	OPD-C	OPDFormer-C	Ours <sub>w/oAL</sub>
OPDReal	16.5	44.5	46.3	<b>51.6</b>
OPDMulti	8.0	25.6	27.6	<b>31.5</b>

	Grounded-SAM	OPDRCNN-C	OPDFormer-C	Ours <sub>w/oAL</sub>	GT
<b>OPDReal</b>					
<b>OPDMulti</b>					

Figure 4. Qualitative results on OPDReal and OPDMulti test set. Ours<sub>w/oAL</sub> outperforms others on noisy GT and multiple objects.

due to imperfect predictions from these models.

As seen in the last two rows of Table 2, using the AL framework, our models show improved performance, reaching over 95% accuracy, with 81.7% time saving in terms of manual effort. The segmentation performance of the two AL methods is close since they share identical network architecture. But they differ in training strategies, impacting labeling efficiency. Specifically, our method is 1 hour faster than Ours<sub>f-AL</sub>, demonstrating the importance of our *coarse-to-fine* AL strategy in minimizing human effort.

**Ablation study.** Table 3 highlights the need and contributions of key components of our method on improving prediction accuracy and minimizing human efforts. Columns 2-5 respectively indicate the presence of: **Obj.** object mask head; **Pos.** pose estimation head; **Dir.** interaction direction prediction head; **AL** active learning. Row 4 uses the *fine* AL stage on part mask alone due to the absence of pose and interaction direction prediction module. Row 5 and 6 use our *coarse-to-fine* AL strategy. Results in Table 3 clearly justify the *coarse-to-fine* design in our method, which gives the best performance (see row 6).

### 6.3. Evaluation on OPDReal and OPDMulti

In addition, we assess the performance of different models on the OPDReal and OPDMulti dataset, using their respective train and test splits. As shown in Table 4, Ours<sub>w/oAL</sub> method outperforms the rest. However, with more than 70% training data, all methods still fail to achieve >55% accuracy on OPDReal. This limitation primarily stems from data



Figure 5. Reconstruct and manipulate bottle and dishwasher

skewness towards the Storage category in OPDReal, which constitutes more than 90% of total samples, and results in poor generalization across other object categories. Detailed category-wise results are provided in the supplementary material. Performance on OPDMulti is further compromised by an abundance of noisy data in its test set[28]. From the qualitative results in Figure 4, we observe that some openable parts are cluttered or missed in the GT annotation, while our method accurately segments these parts. This discrepancy also contributes to the low accuracy.

## 7. Application

Our work demonstrate practical applications in part based reconstruction and manipulation of articulated objects from images. Given a set of multi-view RGB images of an articulated object, our model predicts precise segmentation masks of moveable parts in each image. This enables part based 3D reconstruction using masked images for both moveable parts and the main body of the object. The resulting 3D models of parts allow for easy manipulation of moveable parts to unseen states in 3D as shown in Figure 5.

## 8. Conclusion

We present the first active segmentation framework for high-accuracy instance segmentation of moveable parts in real-world RGB images. Our active learning framework, integrating human feedback, iteratively refines predictions in a *coarse-to-fine* manner, and achieves close-to-error-free performance on the test set. By leveraging correlations between the scene, objects, and parts, we demonstrate that our method can achieve state-of-the-art performance on challenging scenes with multiple cross-categories objects, and significantly reduce human efforts for dataset preparation.

Additionally, we contribute a high-quality and diverse dataset of articulated objects in real-world scene, complete with precise moveable part annotations. We will expand it further to support the vision community for understanding scene from images. We also hope our work catalyzes future motion- or functionality-aware vision tasks.



Figure 6. Qualitative results on *test set* from our dataset. We visualize predictions results on different object categories using 3 competing methods and our final model. Our method outputs better segmentation masks over moveable parts across multiple objects in the image with clear separation of parts and small parts segmentation (Row 1, 4, 5). Our results also show that the *coarse-to-fine* segmentation framework can effectively reduce segmentation errors from unwanted objects (Row 2) and object side surfaces (Row 2, 3, 6, 8). More results in the supplementary materials.



## References

- [1] Trimble Inc. 3D Warehouse. <https://3dwarehouse.sketchup.com/>, 2023. Accessed: 2023-3-4. **3**
- [2] Charu C. Aggarwal, Xiangnan Kong, Quanquan Gu, Jiawei Han, and Philip S. Yu. Active learning: A survey. In *Data Classification: Algorithms and Applications*, pages 571–597. 2014. **2**
- [3] Luca Ballan, Aparna Taneja, Jürgen Gall, Luc Van Gool, and Marc Pollefeys. Motion capture of hands in action using discriminative salient points. In *Computer Vision–ECCV 2012: 12th European Conference on Computer Vision, Florence, Italy, October 7–13, 2012, Proceedings, Part VI 12*, pages 640–653. Springer, 2012. **3**
- [4] Arantxa Casanova, Pedro O Pinheiro, Negar Rostamzadeh, and Christopher J Pal. Reinforced active learning for image segmentation. In *International Conference on Learning Representations*, 2020. **3**
- [5] Angel X Chang, Thomas Funkhouser, Leonidas Guibas, Pat Hanrahan, Qixing Huang, Zimo Li, Silvio Savarese, Manolis Savva, Shuran Song, Hao Su, et al. Shapenet: An information-rich 3d model repository. *arXiv preprint arXiv:1512.03012*, 2015. **3**
- [6] Bowen Cheng, Ishan Misra, Alexander G Schwing, Alexander Kirillov, and Rohit Girdhar. Masked-attention mask transformer for universal image segmentation. In *Proceedings of the IEEE/CVF Conference on Computer Vision and Pattern Recognition*, pages 1290–1299, 2022. **2, 3, 4, 6**
- [7] Alexey Dosovitskiy, Lucas Beyer, Alexander Kolesnikov, Dirk Weissenborn, Xiaohua Zhai, Thomas Unterthiner, Mostafa Dehghani, Matthias Minderer, Georg Heigold, Sylvain Gelly, et al. An image is worth 16x16 words: Transformers for image recognition at scale. In *ICLR*, 2021. **2**
- [8] Grounded-SAM Contributors. Grounded-Segment-Anything, 2023. **3, 6**
- [9] Kaiming He, Georgia Gkioxari, Piotr Dollár, and Ross Girshick. Mask r-cnn. In *Proceedings of the IEEE international conference on computer vision*, pages 2961–2969, 2017. **6**
- [10] Ruizhen Hu, Wenchao Li, Oliver Van Kaick, Ariel Shamir, Hao Zhang, and Hui Huang. Learning to predict part mobility from a single static snapshot. *ACM Transactions on Graphics (TOG)*, 36(6):1–13, 2017. **3**
- [11] Jiahui Huang, He Wang, Tolga Birdal, Minhyuk Sung, Federica Arrigoni, Shi-Min Hu, and Leonidas J Guibas. Multibodysync: Multi-body segmentation and motion estimation via 3d scan synchronization. In *Proceedings of the IEEE/CVF Conference on Computer Vision and Pattern Recognition*, pages 7108–7118, 2021. **2**
- [12] Zeng Huang, Yuanlu Xu, Christoph Lassner, Hao Li, and Tony Tung. Arch: Animatable reconstruction of clothed humans. In *Proceedings of the IEEE/CVF Conference on Computer Vision and Pattern Recognition*, pages 3093–3102, 2020. **3**
- [13] Thomas Jantos, Mohamed Hamdad, Wolfgang Granig, Stephan Weiss, and Jan Steinbrener. PoET: Pose Estimation Transformer for Single-View, Multi-Object 6D Pose Estimation. In *6th Annual Conference on Robot Learning (CoRL 2022)*, 2022. **4**
- [14] Hanxiao Jiang, Yongsen Mao, Manolis Savva, and Angel X Chang. Opd: Single-view 3d openable part detection. In *Computer Vision–ECCV 2022: 17th European Conference, Tel Aviv, Israel, October 23–27, 2022, Proceedings, Part XXXIX*, pages 410–426. Springer, 2022. **2, 3, 5, 6**
- [15] Angjoo Kanazawa, Michael J Black, David W Jacobs, and Jitendra Malik. End-to-end recovery of human shape and pose. In *Proceedings of the IEEE conference on computer vision and pattern recognition*, pages 7122–7131, 2018. **3**
- [16] Alexander Kirillov, Eric Mintun, Nikhila Ravi, Hanzi Mao, Chloe Rolland, Laura Gustafson, Tete Xiao, Spencer Whitehead, Alexander C. Berg, Wan-Yen Lo, Piotr Dollár, and Ross Girshick. Segment anything. *arXiv:2304.02643*, 2023. **2, 3, 6**
- [17] Xiaolong Li, He Wang, Li Yi, Leonidas J Guibas, A Lynn Abbott, and Shuran Song. Category-level articulated object pose estimation. In *Proceedings of the IEEE/CVF Conference on Computer Vision and Pattern Recognition*, pages 3706–3715, 2020. **2**
- [18] Shilong Liu, Zhaoyang Zeng, Tianhe Ren, Feng Li, Hao Zhang, Jie Yang, Chunyuan Li, Jianwei Yang, Hang Su, Jun Zhu, et al. Grounding dino: Marrying dino with grounded pre-training for open-set object detection. *arXiv preprint arXiv:2303.05499*, 2023. **6**
- [19] Siddharth Mahendran, Haider Ali, and René Vidal. 3d pose regression using convolutional neural networks. In *Proceedings of the IEEE International Conference on Computer Vision Workshops*, pages 2174–2182, 2017. **4**
- [20] Dushyant Mehta, Srinath Sridhar, Oleksandr Sotnychenko, Helge Rhodin, Mohammad Shafiei, Hans-Peter Seidel, Weipeng Xu, Dan Casas, and Christian Theobalt. Vnect: Real-time 3d human pose estimation with a single rgb camera. *Acm transactions on graphics (tog)*, 36(4):1–14, 2017. **3**
- [21] Kaichun Mo, Shilin Zhu, Angel X. Chang, Li Yi, Subarna Tripathi, Leonidas J. Guibas, and Hao Su. PartNet: A large-scale benchmark for fine-grained and hierarchical part-level 3D object understanding. In *The IEEE Conference on Computer Vision and Pattern Recognition (CVPR)*, 2019. **3**
- [22] Franziska Mueller, Florian Bernard, Oleksandr Sotnychenko, Dushyant Mehta, Srinath Sridhar, Dan Casas, and Christian Theobalt. GANerated hands for real-time 3d hand tracking from monocular rgb. In *Proceedings of the IEEE conference on computer vision and pattern recognition*, pages 49–59, 2018. **3**
- [23] Munan Ning, Donghuan Lu, Dong Wei, Cheng Bian, Chenglang Yuan, Shuang Yu, Kai Ma, and Yefeng Zheng. Multi-anchor active domain adaptation for semantic segmentation. In *Proceedings of the IEEE/CVF International Conference on Computer Vision*, pages 9112–9122, 2021. **3**
- [24] Pengzhen Ren, Yun Xiao, Xiaojun Chang, Po-Yao Huang, Zhihui Li, Brij B. Gupta, Xiaojiang Chen, and Xin Wang. A survey of deep active learning, 2020. **2**
- [25] Ozan Sener and Silvio Savarese. Active learning for convolutional neural networks: A core-set approach. In *International Conference on Learning Representations*, 2018. **3**
- [26] Gyungin Shin, Weidi Xie, and Samuel Albanie. All you need are a few pixels: Semantic segmentation with pixelpick.

- In *Proceedings of the IEEE/CVF International Conference on Computer Vision (ICCV) Workshops*, pages 1687–1697, 2021.
- [27] Samarth Sinha, Sayna Ebrahimi, and Trevor Darrell. Variational adversarial active learning. In *Proceedings of the IEEE/CVF International Conference on Computer Vision (ICCV)*, 2019. 3
- [28] Xiaohao Sun, Hanxiao Jiang, Manolis Savva, and Angel X. Chang. OPDMulti: Openable part detection for multiple objects. In *Proc. of 3D Vision*, 2024. 2, 3, 5, 6, 7
- [29] Chufeng Tang, Lingxi Xie, Gang Zhang, Xiaopeng Zhang, Qi Tian, and Xiaolin Hu. Active pointly-supervised instance segmentation. In *Computer Vision–ECCV 2022: 17th European Conference, Tel Aviv, Israel, October 23–27, 2022, Proceedings, Part XXVIII*, pages 606–623. Springer, 2022. 2, 3
- [30] Jianyu Wang and Alan L Yuille. Semantic part segmentation using compositional model combining shape and appearance. In *Proceedings of the IEEE conference on computer vision and pattern recognition*, pages 1788–1797, 2015. 3
- [31] Peng Wang, Xiaohui Shen, Zhe Lin, Scott Cohen, Brian Price, and Alan L Yuille. Joint object and part segmentation using deep learned potentials. In *Proceedings of the IEEE International Conference on Computer Vision*, pages 1573–1581, 2015. 3
- [32] Xiaogang Wang, Bin Zhou, Yahao Shi, Xiaowu Chen, Qingping Zhao, and Kai Xu. Shape2motion: Joint analysis of motion parts and attributes from 3d shapes. In *Proceedings of the IEEE/CVF Conference on Computer Vision and Pattern Recognition*, pages 8876–8884, 2019. 3
- [33] Tsung-Han Wu, Yi-Syuan Liou, Shao-Ji Yuan, Hsin-Ying Lee, Tung-I Chen, Kuan-Chih Huang, and Winston H Hsu. D 2 ada: Dynamic density-aware active domain adaptation for semantic segmentation. In *Computer Vision–ECCV 2022: 17th European Conference, Tel Aviv, Israel, October 23–27, 2022, Proceedings, Part XXIX*, pages 449–467. Springer, 2022. 3
- [34] Fangting Xia, Peng Wang, Xianjie Chen, and Alan L Yuille. Joint multi-person pose estimation and semantic part segmentation. In *Proceedings of the IEEE conference on computer vision and pattern recognition*, pages 6769–6778, 2017. 3
- [35] Fanbo Xiang, Yuzhe Qin, Kaichun Mo, Yikuan Xia, Hao Zhu, Fangchen Liu, Minghua Liu, Hanxiao Jiang, Yifu Yuan, He Wang, Li Yi, Angel X. Chang, Leonidas J. Guibas, and Hao Su. SAPIEN: A simulated part-based interactive environment. In *The IEEE Conference on Computer Vision and Pattern Recognition (CVPR)*, 2020. 3, 6
- [36] Binhui Xie, Longhui Yuan, Shuang Li, Chi Harold Liu, and Xinjing Cheng. Towards fewer annotations: Active learning via region impurity and prediction uncertainty for domain adaptive semantic segmentation. In *Proceedings of the IEEE/CVF Conference on Computer Vision and Pattern Recognition*, pages 8068–8078, 2022. 2, 3
- [37] Shuai Xie, Zunlei Feng, Ying Chen, Songtao Sun, Chao Ma, and Mingli Song. Deal: Difficulty-aware active learning for semantic segmentation. In *Proceedings of the Asian Conference on Computer Vision (ACCV)*, 2020. 3
- [38] Zihao Yan, Ruizhen Hu, Xingguang Yan, Luanmin Chen, Oliver Van Kaick, Hao Zhang, and Hui Huang. Rpm-net: recurrent prediction of motion and parts from point cloud. *ACM Transactions on Graphics (TOG)*, 38(6), 2019. 2
- [39] Li Yi, Vladimir G Kim, Duygu Ceylan, I-Chao Shen, Mengyan Yan, Hao Su, Cewu Lu, Qixing Huang, Alla Sheffer, and Leonidas Guibas. A scalable active framework for region annotation in 3d shape collections. *ACM Transactions on Graphics (ToG)*, 35(6):1–12, 2016. 5
- [40] Xueying Zhan, Qingzhong Wang, Kuan-hao Huang, Haoyi Xiong, Dejing Dou, and Antoni B. Chan. A comparative survey of deep active learning, 2022. 2
- [41] Yi Zhou, Connelly Barnes, Jingwan Lu, Jimei Yang, and Hao Li. On the continuity of rotation representations in neural networks. In *Proceedings of the IEEE/CVF Conference on Computer Vision and Pattern Recognition*, pages 5745–5753, 2019. 4
- [42] Xizhou Zhu, Weijie Su, Lewei Lu, Bin Li, Xiaogang Wang, and Jifeng Dai. Deformable detr: Deformable transformers for end-to-end object detection. In *International Conference on Learning Representations*, 2020. 4
- [43] Xueyan Zou, Jianwei Yang, Hao Zhang, Feng Li, Linjie Li, Jianfeng Gao, and Yong Jae Lee. Segment everything everywhere all at once. *arXiv preprint arXiv:2304.06718*, 2023. 3